Journal of Catalysis 257 (2008) 117–124

Contents lists available at ScienceDirect

Journal of Catalysis

www.elsevier.com/locate/jcat

Sintering and redispersion behavior of Pt on Pt/MgO

Toshitaka Tanabe *, Yasutaka Nagai, Kazuhiko Dohmae, Hideo Sobukawa, Hirohumi Shinjoh

Toyota Central R&D Labs., Inc., Nagakute, Aichi-gun, Aichi 480-1192, Japan

ARTICLE INFO

Article history:
Received 14 February 2008
Revised 17 April 2008
Accepted 18 April 2008
Available online 22 May 2008

Keywords:
Platinum
MgO
Redispersion
Regeneration
Sintering
X-ray absorption fine structure
Electron microscopy
Automotive catalyst
Turnover frequency

ABSTRACT

Sintering–redispersion of Pt and deterioration–regeneration of catalytic activity on Pt/MgO as automotive exhaust catalyst were studied. No Pt sintering was observed after air aging up to 1173 K. Pt L_3-edge extended X-ray absorption fine structure results revealed the formation of an Mg_2PtO_4-like compound at the MgO surface and stabilization of oxidized Pt after air aging. Interaction between Pt and MgO involved in the formation of this Mg_2PtO_4-like compound likely provides an anchoring effect that prevents Pt sintering. After redox aging at 1073 K, Pt particles of ca. 20 nm were observed by X-ray diffraction and transmission electron microscopy (TEM). TEM images revealed that sintered Pt redispersed into smaller Pt particles of 2–5 nm on sequential oxidation–reduction treatment at 1073 K. Interactions involved in the formation of the Mg_2PtO_4-like compound should be the driving force for this redispersion. The redispersion behavior led to regeneration of the catalytic activity of Pt/MgO in a simulated automotive exhaust reaction.

1. Introduction

Supported noble metal (Pt, Rh and Pd) catalysts are widely used to control automotive emissions by converting carbon monoxide, hydrocarbons and nitrogen oxides to carbon dioxide, water and nitrogen in the exhaust gas [1,2]. Deterioration of catalytic activity is one of the main problems in maintaining low emissions during automotive life. The noble metal loading is thus designed to provide sufficient catalytic performance to maintain low emission levels even after deterioration with long-term usage. If catalyst deterioration can be improved, the noble metal loading can be decreased, leading to more efficient use of natural resources. One of the main causes of deterioration is sintering of the supported noble metals in the catalyst [3–12]. Because Pt easily agglomerates at high temperature (above ca. 1023 K) in the presence of oxygen [4,5], inhibition of Pt sintering is one of the key issues in developing efficient automotive catalysts with low Pt loading. In the last two decades, the mechanism of Pt sintering has been investigated extensively with experimental techniques [4–8,10] and modeling work [8,9,11,12]. Flynn and Wanke developed a model of supported Pt sintering based on the molecular migration of Pt along the surface [8,9]. In that model, single atoms or molecular cluster escaped from the particles, moved along the surface and were captured by other particles. Through this process the particle size increased and the total surface area of Pt decreased. Dadyburjor et al. also proposed a similar model, but suggested that the internal stress in the Pt particle might have an effect on the multi atom escape from the Pt particle [11,12]. Völter et al. showed experimentally that the species migrating on the support surface should be oxidized Pt species [10]. This kind of species has been also suggested by Flynn and Wanke [8]. Based on these studies, the more severe Pt sintering observed in oxidative atmospheres should be caused by the production of oxidized Pt species that migrate on the support surface. Besides sintering, the redispersion of supported noble metals has also been studied for a long period. An oxy-chlorination treatment was effective for Pt redispersion and used to regenerate catalytic activity of supported Pt catalysts [13–19]. In those studies, oxy-chlorination was needed to oxidize the Pt crystallites and produce the mobile species including Pt [16,19]. The oxidized Pt species were deduced by in situ X-ray absorption spectroscopy to be a complex containing oxygen and chlorine [17]. In this redispersion process, that mobile species migrated and were trapped on support sites and decomposed to smaller Pt particles. Redispersion of noble metals on supported catalysts in oxidative atmospheres was also reported in some papers [20–30]. Baker at al. showed the redispersion of sintered Ir on Al_2O_3 via the formation of iridates with Group IIA-oxides [20]. They proposed that redispersion proceeded with the capture of mobile, molecular iridium oxide species by Group IIA-oxides on the support surface. Nishihata et al. studied on $LaFe_{0.57}Co_{0.38}Pd_{0.05}O_3$ perovskite-based catalysts with X-ray diffraction and absorption [21]. They suggested the reversible movement of Pd into and out of the perovskite lattice in

* Corresponding author. Fax: +81 561 63 6150.
E-mail address: t-tanabe@mosk.tytlabs.co.jp (T. Tanabe).

0021-9517/$ – see front matter
doi:10.1016/j.jcat.2008.04.012

oxidative and reductive atmosphere cycles that were likely responsible for the high durability of this catalyst and called this phenomenon self-regeneration. Concerning Pt, the redispersion under oxidative atmosphere was reported mainly on Pt/Al_2O_3 catalysts with moderate treatment temperature of around 773 K [22–31]. Pt redispersion under oxidative atmosphere is closely connected to sintering phenomena. Wanke et al. showed that oxidative atmosphere treatment of Pt/Al_2O_3 at 823 K caused Pt redispersion and higher temperature than 873 K caused Pt sintering. They proposed a molecular migration mechanism of oxidized Pt for Pt sintering and redispersion in Pt/Al_2O_3 [22]. In this mechanism, the oxidized species migrated on the surface and were trapped at surface sites in redispersion or were captured in Pt crystallites in sintering. Some experimental studies showed that oxidized Pt was stabilized by forming a complex with the Al_2O_3 support in redispersion [23,26]. Although slightly different mechanisms were proposed, e.g. oxide film formation [28,29] or particles splitting model [30,31] for redispersion, the molecular migration and trapped oxidized Pt species on surface sites was common [22–27]. Based on this mechanism, oxidation of Pt and the interaction between oxidized Pt and the support surface sites are important for redispersion.

Nagai et al. recently investigated the interaction between Pt and the support oxide in terms of the inhibition mechanism for Pt on ceria-based oxides [32]. The authors reported that the interaction between Pt and the support oxide inhibited Pt sintering at 1073 K under oxidizing conditions, and that the oxygen 1s core electron level in the support oxide was important for this interaction. The oxidized Pt stabilization was observed on oxides with a lower oxygen 1s core electron level. This oxidized Pt had strong interaction with support and this interaction inhibited the Pt sintering. The oxygen 1s core electron level correlates with the electron density on oxygen and the low core electron level corresponds to high electron density [33]. Higher electron density on oxygen means more electron localization on oxygen rather than covalency. This trend is usually discussed with electronegativity of the element and the acid–base properties of oxide. So, low oxygen 1s core electron level corresponds to more basic property of oxides with lower electronegativity cations. The stabilization of oxidized Pt on basic oxides was already reported and discussed in terms of electronegativity [34]. From this viewpoint, oxygen core electron level should be an experimental parameter to describe the acid–base oxide property and have parallelism with electronegativity. In the present study, we attempted to regenerate the activity of an aged Pt catalyst by redispersion of sintered Pt using the interaction between Pt and the support oxide at high temperature mentioned above. A typical basic oxide (MgO) was chosen as the support because more basic cation in the oxide has a lower oxygen 1s core electron level [32], for which a stronger interaction is expected. MgO is also favorable as a support oxide because of its high surface area. γ-Al_2O_3 was also investigated for comparison. Although Pt redispersion was observed on Al_2O_3 at moderate temperature, it is thought to interact weakly with Pt at high temperature [22,32]. Comparative investigation of these two oxides should provide some insights into the role of the interaction between Pt and the support oxide for Pt redispersion.

2. Experimental

2.1. Catalyst preparation and aging tests

Pt/MgO and Pt/γ-Al_2O_3 were prepared by the usual impregnation method. MgO (Ube Material Industries) and γ-Al_2O_3 (Nikki Universal) were impregnated with $Pt(NH_3)_2(NO_2)_2$ (Tanaka Kikinzoku Kogyo K.K.). The impregnated catalyst was dried in an oven at 383 K for 24 h and calcined in flowing air at 773 K for 5 h. The Pt loading was controlled at 1 wt%. The catalyst powders were pressed into disks, crushed and sieved to yield pellets of 0.5–1.0 mm for aging and catalytic reaction tests.

Aging tests were performed under two atmospheric conditions. In one aging test, catalyst pellets were placed in a quartz tube and heated at 973, 1073 or 1173 K for 5 h in an air flow (hereafter referred as the air aging test). In the other test, catalyst pellets were placed in a quartz tube and heated at 1073, 1173 or 1273 K for 5 h in a flow cyclically switched every 5 min between 5% O_2 in N_2 and 10% H_2 in N_2 (referred to as the redox aging test). The total flow rate was controlled at 1 L/min in both aging tests.

2.2. Characterization

X-ray diffraction (XRD) was used to evaluate the Pt particle size in each catalyst after aging tests. Measurements were performed using a Rigaku SX instrument with Co $K\alpha$ radiation ($\lambda = 1.7903$ Å) operated at 30 kV and 30 mA at a scan speed of 0.125 deg/min. The particle size was estimated from the width at half-height (β) of the XRD line of Pt(311) using the Scherrer equation $L = K\lambda/\beta\cos\theta$ ($K = 1$, $\lambda = 1.7903$ Å).

The Pt dispersion was determined by CO pulse chemisorption at 323 K using an Ohkura Riken R6015-S instrument. The sample was heated to 673 K in flowing O_2 and held at this temperature for 15 min. After purging with He, the sample was reduced in H_2 for 15 min and then cooled to 323 K in flowing He. A CO pulse was injected into the sample at 323 K until the adsorption reached saturation. The amount of CO adsorbed was calculated as the difference between total amount of CO injected and the outlet from the sample. Metal dispersion was calculated by assuming a CO/surface Pt atom ratio of 1:1 [35].

Transmission electron microscopy (TEM) was performed on a JEOL JEM2000-EX system at an acceleration voltage of 200 kV to observe Pt particles in the catalysts.

Pt L_3-edge (11.5 keV) X-ray absorption fine structure (XAFS) measurements were carried out using the BL01B1 and BL16B2 beamlines at the SPring-8 facility (Hyogo, Japan) to investigate the local coordination structure around Pt and its chemical state after aging tests. Standard samples of Pt foil and PtO_2 were also measured as references for Pt metal and Pt oxide. The storage ring energy was operated at 8 GeV with a typical current of 100 mA. XAFS spectra at the Pt L_3-edge were measured using a Si(111) double-crystal monochromator in transmission mode at room temperature in air. XAFS data reduction was carried out as described elsewhere [36]. Curve-fitting analysis of extended XAFS (EXAFS) spectra was performed for inverse Fourier transforms on the Pt-oxygen and Pt-cation (cations Pt and Mg) shells using theoretical parameters calculated by McKale et al. [37].

X-ray photoelectron spectroscopy (XPS) measurements were carried out using a PHI model 5500MC instrument with Mg $K\alpha$ radiation. Oxygen 1s core electron levels in the support oxides were recorded to evaluate the chemical properties of the support. Binding energies were calibrated with respect to Pt $4f_{7/2}$ at 71.4 eV [32]. The spectrum of Pt $4f_{7/2}$ was also measured to evaluate the valence state of Pt. To calculate the proportion of each valence state, spectral deconvolution was performed.

2.3. Catalytic reaction test

Catalytic reaction tests were carried out in a tubular fixed-bed reactor at atmospheric pressure with a simulated automotive exhaust gas using a conventional flow system [38]. A quantity of 1.0 g of catalyst was used and the total flow rate was 3.3 L/min ($W/F = 0.009$ g s mL^{-1}). The conversion of hydrocarbon (HC), carbon monoxide (CO) and NO_x over the catalysts was measured as a function of temperature between 373 and 773 K using a simulated exhaust gas containing 0.7% CO, 0.23% H_2, 0.053% C_3H_6, 0.12% NO,

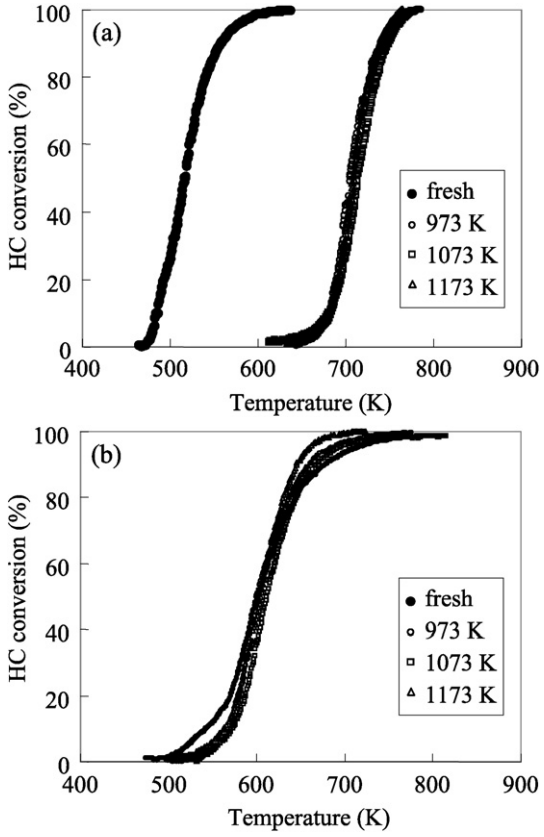

Fig. 1. Temperature dependences of hydrocarbon conversion in simulated exhaust reactions over fresh and air aged catalysts. (a) Pt/γ-Al_2O_3, (b) Pt/MgO. Air aging temperature: 973, 1073 or 1173 K.

0.646% O_2, 10% CO_2, and 3% H_2O in N_2. This gas composition resembles the exhaust gas of a gasoline fueled automotive internal combustion engine operating under a stoichiometric air/fuel ratio. Samples were pretreated in situ in the simulated exhaust gas at 773 K for 15 min and then cooled to 373 K before catalytic reaction tests. The concentrations of HC, CO and NO_x in the outlet were measured using an exhaust gas analysis system (MEXA8120, Horiba) as a function of the reaction temperature.

3. Results and discussion

3.1. Air aging

Since previous work [32] revealed that interaction between Pt and the support oxide should occur under oxidizing conditions, the effect of air aging on the catalyst was investigated as a first step. Fig. 1 shows the temperature dependences of HC conversion for Pt/γ-Al_2O_3 in (a) and Pt/MgO in (b), before and after air aging tests at 973, 1073 and 1173 K. The catalytic activity of Pt/γ-Al_2O_3 deteriorated severely after air aging tests while the activity of Pt/MgO changed little. As the characteristic temperature dependence of the catalytic reaction in automotive exhaust, the conversion showed very sharp increase in a narrow temperature region and shifted to higher temperature after aging. To evaluate this kind of catalytic activity, the temperature at which 50% HC conversion occurs (referred as T_{50}) has been frequently used as the indicator of catalytic activity [15] and chosen also in this work. Thus, HC conversion reaches 50% at T_{50} and a lower value of T_{50} indicates higher catalytic activity. Fig. 2 shows T_{50} values for Pt/γ-Al_2O_3 and Pt/MgO, before and after air aging tests at 973, 1073 and 1173 K. T_{50} for Pt/MgO did not change, whereas T_{50} for Pt/γ-Al_2O_3 increased by approximately 200 K after air aging tests. This result indicates that

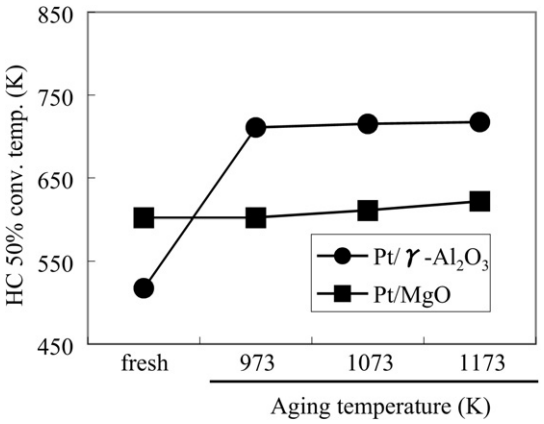

Fig. 2. Hydrocarbon 50% conversion temperatures (T_{50}) in simulated exhaust reactions over Pt/MgO and Pt/γ-Al_2O_3 before and after air aging tests.

Table 1
Pt particle size determined by XRD in Pt/γ-Al_2O_3 and Pt/MgO after air aging test

Aging temperature (K)	Pt particle size (nm)	
	Pt/γ-Al_2O_3	Pt/MgO
973	30	N.D.
1073	34	N.D.
1173	35	N.D.

Note. N.D.: not detected.

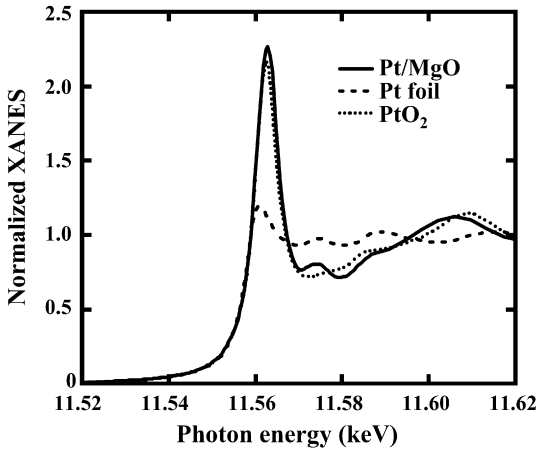

Fig. 3. Pt L_3-edge XANES spectra of Pt/MgO after 1073 K air aging test, together with standard samples of Pt foil and PtO_2 powder.

Pt/MgO had higher stability than Pt/γ-Al_2O_3 under oxidizing conditions at high temperature, although its catalytic activity was not as high as that of Pt/γ-Al_2O_3 before the aging test.

The Pt particle size in Pt/MgO and Pt/γ-Al_2O_3 determined by XRD measurements after air aging tests is shown in Table 1. No Pt sintering was observed in Pt/MgO, although the Pt particle size in Pt/γ-Al_2O_3 was ca. 30 nm. The oxygen 1s binding energy measured by XPS for MgO and γ-Al_2O_3 was 529.6 and 531.4 eV, respectively. According to these XPS results, the stability of Pt against sintering agreed with previous results in terms of the oxygen 1s core electron level [32]. This stability of Pt on MgO against sintering corresponded to the stable catalytic performance of Pt/MgO after air aging tests.

To investigate the state of Pt in Pt/MgO after air aging tests, XAFS measurements were performed. Fig. 3 shows the X-ray absorption near edge structure (XANES) spectra at L_3-edge for Pt/MgO after air aging at 1073 K with the spectra of standard samples of Pt foil and PtO_2. In the case of Pt L-edge XANES, the

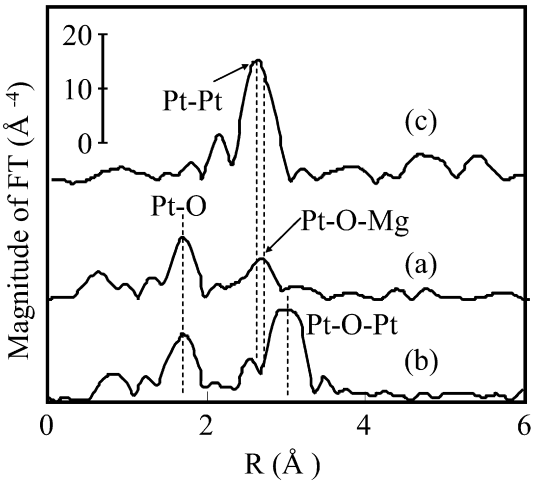

Fig. 4. Fourier-transformed spectra of Pt L_3-edge EXAFS for (a) Pt/MgO after 1073 K air aging tests, and standard samples of (b) PtO_2 powder and (c) Pt foil.

Table 2
Results of curve-fitting analysis for the Pt/MgO after 1073 K air aging test and the standard samples

Sample	Shell	CN	R (Å)	σ^2 (Å^2)
Pt foil[a]	Pt–Pt	12.0	2.76	0.0045
Pt/MgO	Pt–O	5.9	2.04	0.0041
	Pt–Mg	6.2	3.02	0.0027
PtO_2[a]	Pt–O	5.7	2.04	0.0026
	Pt–Pt	5.3	3.10	0.0019

Note. CN, coordination number; R, bond distance; σ, Debye–Waller factor.
[a] The curve-fitting analysis for the standard samples was performed by references to [41,42].

white line absorption intensity reflects the vacancy of Pt 5d orbital [39] and is used to estimate the Pt oxidation state [40]. The white line absorption intensity of Pt/MgO after air aging at 1073 K showed comparable or even higher intensity than standard sample of PtO_2. This result indicated that Pt existed in the Pt^{4+} oxidation state in Pt/MgO after air aging at 1073 K. Fig. 4 shows the Fourier-transformed Pt L_3-edge EXAFS spectrum for Pt/MgO after air aging at 1073 K, with spectra of standard samples of Pt foil and PtO_2 shown as references for bulk Pt metal and Pt oxide. Quantitative curve-fitting analysis of the EXAFS spectra was performed for inverse Fourier transforms on the Pt-oxygen and Pt-cation (cation = Pt and Mg) shells. The results of curve-fitting were summarized in Table 2. The FTs are not corrected for phase shift; therefore, the peaks in the FTs are shifted to lower R values. The values of bond length in the text and table are corrected for phase shift. In the FT spectrum of Pt foil, the peak at 2.76 Å is assigned to the Pt–Pt bond. In the FT spectrum of PtO_2, the peaks at 2.04 and 3.10 Å are assigned to the Pt–O and Pt–O–Pt bonds, respectively. The spectrum of Pt/MgO is clearly different from that of bulk Pt foil and PtO_2. No peak corresponding to the Pt–Pt bond, which should appear at 2.76 Å, was observed in the EXAFS spectrum of Pt/MgO after air aging at 1073 K. The first peak at 2.04 Å was close to that of PtO_2 and it was fitted with the Pt–O bond. The second evident peak at 3.02 Å was not observed in both Pt foil and PtO_2. A curve-fitting simulation of this second peak was carefully performed. Fig. 5 shows the results based on the supposition that the second neighboring atom was Mg or Pt. An excellent fitting result for the simulation of Mg was obtained. In contrast, an appropriate fit could not be obtained for Pt, because the EXAFS oscillation pattern of Pt was very different than that of the experimental data. From this fitting, this second peak was assigned to Pt–O–Mg bond with a distance of 3.02 Å and its coordination number (CN) was 6.2. These XANES and EXAFS results on Pt/MgO after air aging tests at 1073 K indicated that Pt was dispersed at the atomic level as Pt^{4+} and was surrounded by six oxygen atoms in Pt/MgO and that its state was different from that of bulk PtO_2. Muller et al. reported that PtO_2 reacts with MgO to form an inverse spinel-type oxide of Mg_2PtO_4 at an oxygen pressure of 150–200 atm at 1123 and 1173 K [43]. Such a high oxygen pressure was needed to stabilize oxidized Pt because PtO_2 is easily reduced to the metallic state above 900 K in air. In this inverse spinel structure, Pt is surrounded by six oxygen atoms at octahedral sites. Asakura et al. reported an Pt L_3-edge EXAFS analysis on Pt/MgO catalyst [44], in which the very similar values for Pt local structure were found; the first neighbor was Pt–O with 2.03 Å distance and CN = 6.2, the second neighbor was Pt–Mg (oct) with 3.01 Å distance and CN = 6.0 and third neighbor was Pt–Mg (tetra) with 3.45 Å distance and CN = 4.0. They discussed these results on the basis of a formation of spinel type oxide of Mg_2PtO_4 and proposed that Pt^{4+} ion substituted for Mg^{2+} in the top layer of MgO lattice and its structure distorted to this spinel-like structure. Based on the literature and present XAFS results, we concluded that Pt reacted with MgO to form an Mg_2PtO_4-like compound in air aging tests and existed as atomically dispersed Pt^{4+} ions than sintered metallic Pt particles. The formation of a binary oxide including Pt in supported catalysts was already proposed by Yoshida et al. [34]. They discussed Pt L_3-edge XANES results with thermochemical data and showed that electrophobic oxides, such as alkali and alkaline earth oxides, promote noble metal oxidation and the formation of binary oxides including noble metal. The present re-

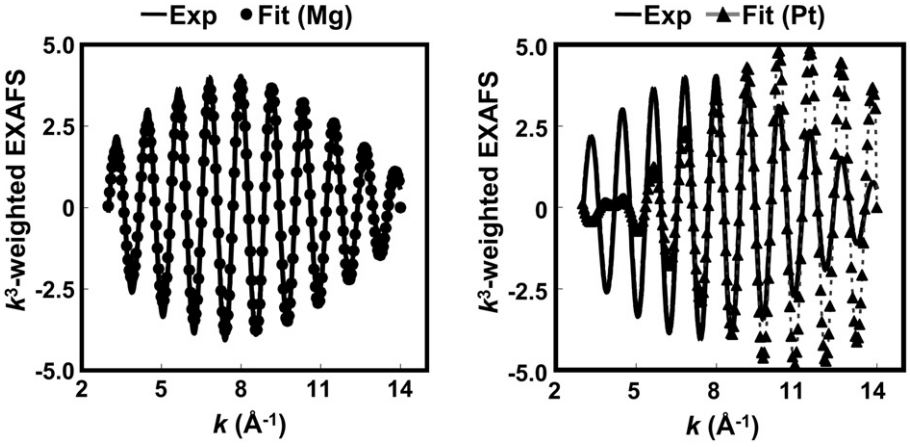

Fig. 5. Curve-fitting analysis on the inverse Fourier-transform of the second peak on the Pt/MgO after 1073 K air aging test in Fig. 4 and the corresponding curve fit. (Left) Experimental (—) and curve-fit on Mg atom (●). (Right) Experimental (—) and curve fit on Pt atom (--▲--).

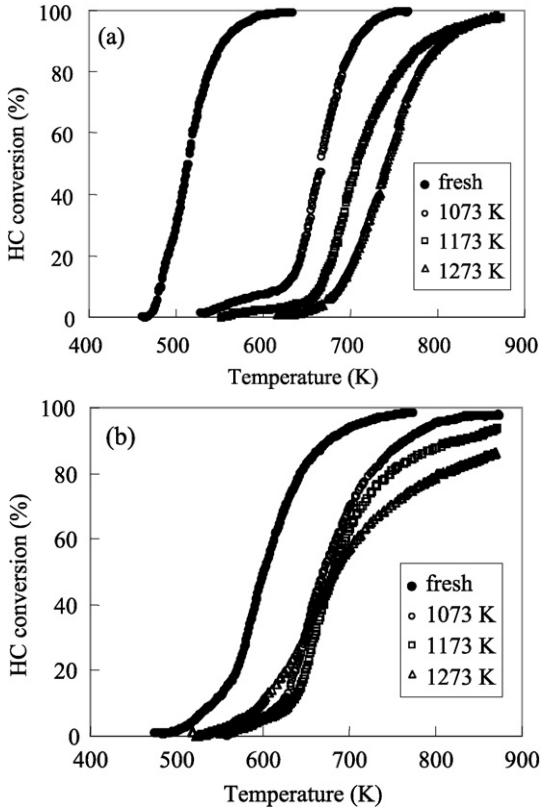

Fig. 6. The temperature dependences of hydrocarbon conversion in simulated exhaust reactions over fresh and redox aged catalysts. (a) Pt/γ-Al_2O_3, (b) Pt/MgO. Redox aging temperature: 1073, 1173 or 1273 K.

sults and conclusion agree with that proposed mechanism since MgO is a typical electrophobic oxide. This Mg_2PtO_4-like compound is considered to be restricted to the MgO surface [44], because its formation starts on the MgO surface and the Mg/Pt atomic ratio (>2) was much too great for bulk Mg_2PtO_4. The formation of this Mg_2PtO_4-like compound should act as an anchor for Pt at the MgO surface and should be responsible for inhibiting Pt sintering in air aging tests.

3.2. Redox aging

In real situations, automotive catalysts are exposed not only to oxidizing, but also to reducing conditions, because combustion is controlled at a stoichiometric condition between oxidizing and reducing atmospheres to achieve highly efficient catalytic purification of the exhaust gas [1,2]. To simulate this situation, redox aging tests were performed. The temperature dependences of HC conversion are shown in Fig. 6 for Pt/γ-Al_2O_3 in (a) and Pt/MgO in (b), before and after air aging tests at 1073, 1173 and 1273 K. The conversion curve of Pt/γ-Al_2O_3 shifted almost monotonously to higher temperature with increase of redox aging temperature. In the case of Pt/MgO, although the conversion curve of the aged catalyst shifted to higher temperature from that of fresh catalyst, the changes within the aged catalysts were not as simple as that of Pt/γ-Al_2O_3. The temperature dependence of conversion of the catalyst aged at 1273 K was less steep than those of other aged catalysts. At lower reaction temperature, Pt/MgO aged at 1273 K showed higher activity than those aged at 1173 or 1073 K. The conversion increased less steeply than other aged catalysts and showed lower activity at high reaction temperature. T_{50} for HC conversions after redox aging tests at 1073, 1173 and 1273 K are shown in Fig. 7 for the comparison of catalytic activity. In contrast to air aging tests, T_{50} for Pt/MgO increased after

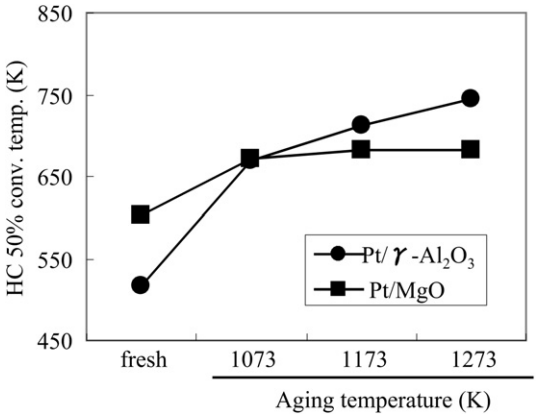

Fig. 7. Hydrocarbon 50% conversion temperatures (T_{50}) in simulated exhaust reactions over Pt/MgO and Pt/γ-Al_2O_3 before and after redox aging tests.

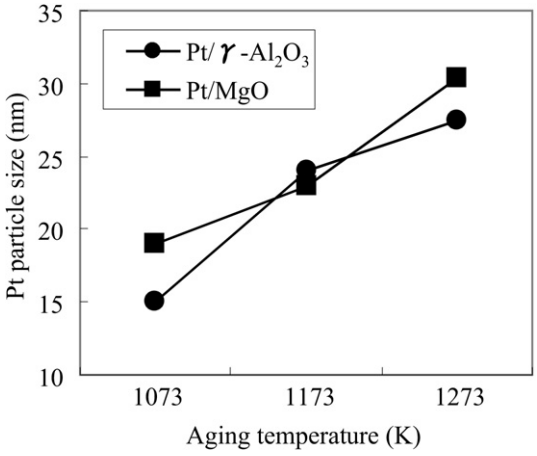

Fig. 8. Particle size of Pt in Pt/MgO and Pt/γ-Al_2O_3 determined by XRD after redox aging tests.

redox tests, although it did not depend on the aging temperature. Pt/MgO showed comparable catalytic activity to that of Pt/γ-Al_2O_3 after redox aging tests at 1073 K. After redox tests at 1173 and 1273 K, Pt/MgO showed higher catalytic activity than Pt/γ-Al_2O_3. This trend was the same if the overall conversion curve was compared among these catalysts. XRD measurements revealed sintered Pt in both catalysts after redox aging, as shown in Fig. 8. The Pt particle size in both catalysts increased with the aging temperature, and the Pt particle size was comparable in Pt/MgO and Pt/γ-Al_2O_3 after redox aging tests at all temperature. These XRD results are not consistent with the catalytic activity results in the viewpoints of the difference between Pt/γ-Al_2O_3 and Pt/MgO, and also the aging temperature dependence of Pt/MgO.

To investigate this discrepancy in more detail, CO pulse adsorption measurements were used. The Pt dispersions determined by this method are shown in Fig. 9. Pt dispersion in Pt/MgO was almost constant after the redox aging tests. After redox aging at 1073 K, the Pt dispersion in Pt/MgO was comparable to that of Pt/γ-Al_2O_3. After redox tests at 1173 and 1273 K, the Pt dispersion in Pt/MgO was greater than that in Pt/γ-Al_2O_3. This trend for Pt dispersion after redox aging tests is fairly consistent with the catalytic activity. Because Pt dispersion is considered to be a direct measure of the number of active sites in the Pt-supported catalyst, the higher Pt dispersion in Pt/MgO should be responsible for its higher catalytic activity compared to Pt/γ-Al_2O_3. Using these Pt dispersion results, turnover frequency (TOF) of these catalysts was estimated at a reaction temperature of 673 K. The temperature of 673 K was chosen because that temperature was necessary to get

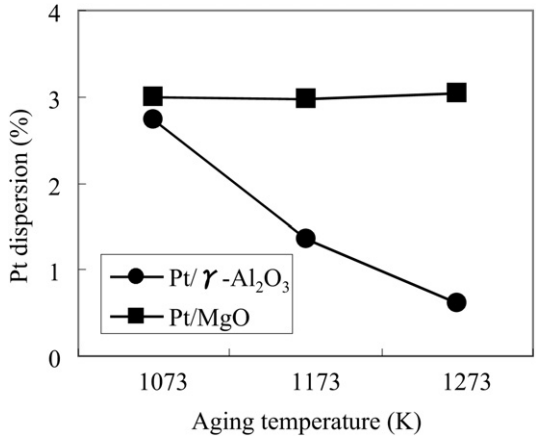

Fig. 9. Dispersions of Pt in Pt/MgO and Pt/γ-Al_2O_3 determined by CO pulse adsorption after redox aging tests.

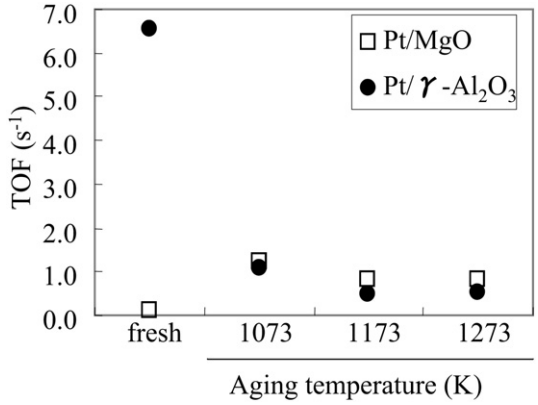

Fig. 10. Turn over frequencies (TOF) of fresh and redox aged Pt/γ-Al_2O_3 and Pt/MgO. TOF was estimated at 673 K reaction temperature. The values for Pt/γ-Al_2O_3 aged at 1173 and 1273 K were experimental and for others were estimated from the conversions at lower temperature with an assumption of Arrhenius-type temperature dependence. Pt dispersions in Fig. 9 were used for aged catalysts. Pt dispersion of fresh Pt/γ-Al_2O_3 and Pt/MgO determined by CO pulse adsorption were 55 and 21%, respectively and used to estimate the TOFs of fresh catalysts.

enough conversion with Pt/γ-Al_2O_3 redox aged at 1273 K, which showed the lowest activity. The conversions over some catalysts, especially the fresh catalysts, were too high at 673 K to estimate TOF. In such a case, the TOF was estimated from the extrapolation of the conversions at lower temperature with an assumption of Arrhenius-type temperature dependence. The Pt dispersions of fresh Pt/γ-Al_2O_3 and Pt/MgO were determined as 55 and 21%, respectively by CO pulse adsorption and used to estimate the TOF of fresh catalysts. The results are shown in Fig. 10. The TOF of fresh Pt/γ-Al_2O_3 was much higher than that of fresh Pt/MgO. TOF of Pt/γ-Al_2O_3 decreased and that of Pt/MgO increased after redox aging. The TOFs of redox aged catalysts were almost the same among six Pt/γ-Al_2O_3 and Pt/MgO catalysts. The large TOF difference between fresh Pt/γ-Al_2O_3 and Pt/MgO is likely caused by a support effect on the fresh catalyst. The catalyst on the more basic support showed lower activity for hydrocarbon oxidation and this effect was attributed to the stabilization of oxidized Pt on the oxide [34]. After aging tests, the TOFs of the aged catalysts were almost the same regardless of the support or the Pt particle size. This means that the reaction was structure-insensitive.

The discrepancy between the Pt particle size determined by XRD and the Pt dispersion determined by CO adsorption should be attributed to the difference in Pt particle size distribution in these catalysts, because the experimental results give only an average value over the distribution. The number of Pt particles smaller

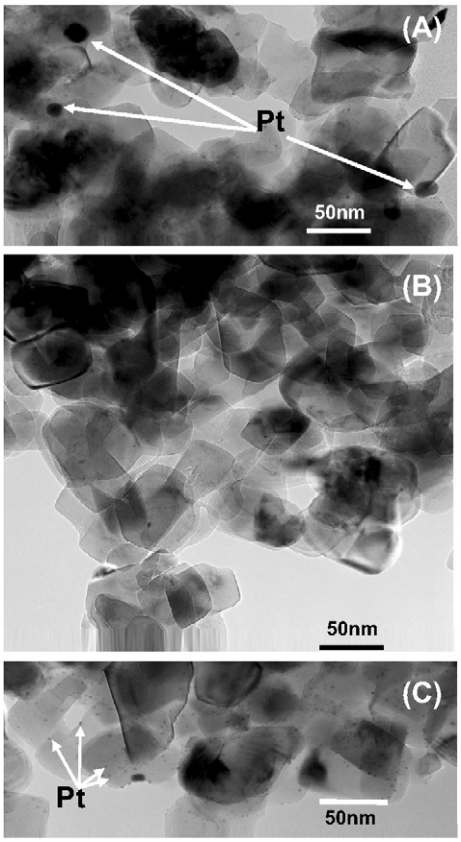

Fig. 11. TEM image of Pt/MgO (A) after a redox aging test at 1073 K, (B) after thermal treatment at 1073 K in air for 5 h and (C) after reduction at 1073 K for 5 h in 10% H_2/N_2.

than ca. 5 nm, which are not observable by XRD measurement, should be greater on Pt/MgO than on Pt/γ-Al_2O_3. These small Pt particles contribute to the CO adsorption and catalytic activity. The larger number of small Pt particles on Pt/MgO could be caused by strong interaction between Pt and MgO under oxidizing conditions, as mentioned in Section 3.1. Even among the aged Pt/MgO, the Pt particle size estimated by XRD increased with increasing aging temperature although the Pt dispersions were almost constant after any aging temperature. This result would indicate the Pt particle size distribution change in Pt/MgO with increasing aging temperature. A bimodal type distribution would account for these results [25], in which the large Pt particles sintered to larger particles and the number of Pt particles smaller than ca. 5 nm increased with increasing aging temperature. This Pt particle size distribution change might be a reason for the change of the temperature dependence of the conversion of aged Pt/MgO.

3.3. Regeneration after redox aging

If the interaction between Pt and MgO under oxidizing conditions is effective after redox aging of samples, this interaction could be a driving force for the redispersion of sintered Pt particles. Thermal treatment in air at 1073 K could cause a reaction between Pt particles and MgO to form an Mg_2PtO_4-like compound on the MgO surface. This reaction could cause atomic-level redispersion of Pt on the MgO surface under oxidizing conditions. To investigate this hypothesis, Pt/MgO was submitted to a redox aging test at 1073 K, after which it was treated in air for 5 h at 1073 K. The catalyst was then reduced in a flow of 10% of H_2 in N_2 for 5 h at 1073 K. The size of the Pt particles after each treatment was investigated by TEM and XRD. TEM images of the catalyst after each treatment are shown in Fig. 11. After the redox aging test, Pt par-

Table 3
The percentage of high valence state Pt (Pt^{2+}, Pt^{4+}) after each treatment

Sample	(A)	(B)	(C)
Pt/MgO	60%	80%	30%
Pt/γ-Al_2O_3	0%	0%	0%

Note. (A) Aged at 1073 K in redox cycle, (B) after thermal treatment at 1073 K in air and (C) after reduction at 1073 K in H_2/N_2 sample B.

ticles of ca. 20 nm were observed in TEM images (Fig. 11A), which is comparable to the size estimated from XRD measurements. After thermal treatment in air at 1073 K, large Pt particles almost disappeared (Fig. 11B) and no Pt diffraction peak was observed in the XRD pattern. After this oxidizing treatment, Pt particles were considered to have been redispersed at the atomic level, with the formation of Mg_2PtO_4-like compound on the MgO surface. After reduction by 10% H_2/N_2 at 1073 K, many Pt particles of 2–5 nm appeared (Fig. 11C). After this reducing treatment, Pt atoms segregated as metallic Pt particles from the Mg_2PtO_4-like compound. These results demonstrated that sequential oxidation and reduction treatments at 1073 K led to redispersion of sintered Pt into smaller Pt particles, and the interaction between Pt and MgO was effective at high temperature, even after redox aging tests. During this sequential treatment, the oxidation state of the supported Pt was investigated by XPS. Pt/γ-Al_2O_3 was also investigated for comparison. XPS measurements were made on both samples after redox aging tests, oxidizing treatment and reducing treatment. The percentage of Pt in high valence states (summation of Pt^{2+} and Pt^{4+}) is summarized in Table 3. On Pt/γ-Al_2O_3, supported Pt was found to be in the Pt^0 (metallic) state after every treatment, and no high valence state was observed. Because Pt was sintered as large particles on Pt/γ-Al_2O_3 after redox aging tests, almost all the Pt atoms should exist as large Pt particles in the metallic state. On the other hand, a high valence state (Pt^{2+} or Pt^{4+}) was observed on Pt/MgO, even after redox aging, although large Pt particles were confirmed both in TEM images and from XRD measurements. This result suggests that some Pt atoms interacted strongly with MgO and not all Pt atoms existed as large particles, even after redox aging. The percentage of Pt in high valence states increased to 80% after oxidizing treatment and decreased to 30% after reducing treatment. A proportion of Pt after reducing treatment could be transformed to high valence states during sample transfer in air at room temperature for XPS measurements. The present redispersion results agreed well with the redispersion mechanism [22–27] in which oxidized Pt species migrated along surface and were trapped at surface sites. The XPS observation of a high valence state Pt in Pt/MgO after oxidizing treatment revealed the presence of oxidized Pt species in the redispersion. The Mg_2PtO_4-like compound should be the trap site for oxidized Pt species and should be a driving force for the redispersion.

To determine if the regeneration of catalytic activity can be attributed to this Pt redispersion, a catalytic activity test was performed on Pt/MgO using a simulated exhaust gas. For comparison, Pt/γ-Al_2O_3 was treated in the same manner and its catalytic activity was also tested. Fig. 12 shows T_{50} for the catalytic reaction. As mentioned in Section 3.2, Pt/γ-Al_2O_3 showed much higher activity than Pt/MgO before aging. T_{50} for both Pt/MgO and Pt/γ-Al_2O_3 increased to comparable values after the redox aging test. T_{50} for Pt/MgO decreased after sequential oxidation–reduction treatment at 1073 K after redox aging tests, whereas T_{50} for Pt/γ-Al_2O_3 increased further. Since the number of active sites dominantly determined catalytic activity after redox aging tests mentioned in Section 3.2, this catalytic regeneration was considered to be caused by the redispersion of Pt. These results demonstrated that deactivated Pt in Pt/MgO catalyst could be regenerated via redispersion of the agglomerates by sequential oxidation–reduction treatment at 1073 K, whereas the activity of Pt/γ-Al_2O_3 further deteriorated after the same treatment. The results indicate that a strong interaction between Pt and the support oxide is essential for catalyst regeneration.

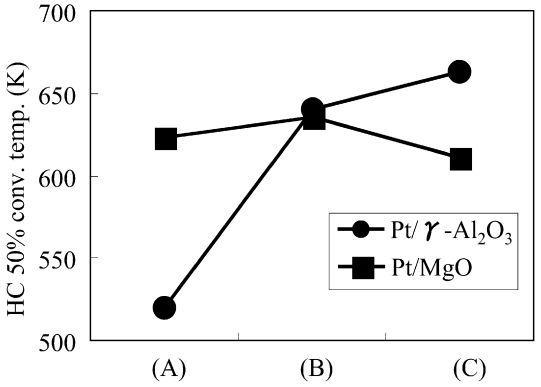

Fig. 12. Hydrocarbon 50% conversion temperatures (T_{50}) in simulated exhaust reactions over Pt/MgO and Pt/γ-Al_2O_3: (A) before aging; (B) after a redox aging test at 1073 K; and (C) after sequential oxidation for 5 h in air and reduction for 5 h in 10% H_2/N_2 at 1073 K.

4. Conclusions

After redox aging tests at above 1073 K, the catalytic activity of Pt/MgO deteriorated and Pt agglomerates of ca. 20 nm were observed by XRD and TEM. TEM images revealed that the sintered Pt redispersed into smaller particles of 2–5 nm on sequential treatment in 20% O_2/N_2 followed by 5% H_2/N_2 at 1073 K. This redispersion of Pt led to regeneration of the catalytic activity of Pt/MgO to a value almost the same as that before the aging test. In contrast the same sequential treatment caused further deterioration of Pt/γ-Al_2O_3 after redox aging at 1073 K. EXAFS and XPS results revealed oxidized Pt species and the formation of Mg_2PtO_4-like compound on the MgO surface after oxidizing treatment at 1073 K. This Mg_2PtO_4-like compound formation should be the driving force for the redispersion.

Acknowledgments

We thank Mr. N. Suzuki for TEM observations, Mr. N. Isomura for XPS measurements, and Mr. N. Takahashi for fruitful discussions.

References

[1] S. Matsumoto, Catal. Today 90 (2004) 183.
[2] H.C. Yao, Y.F. Yao, J. Catal. 86 (1984) 254.
[3] C.H. Bartholomew, Appl. Catal. A Gen. 212 (2001) 17.
[4] R.M.J. Fiedorow, B.S. Chahar, S.E. Wanke, J. Catal. 51 (1978) 193.
[5] S.A. Hassan, F.H. Khalil, F.G. El-Gamal, J. Catal. 44 (1976) 5.
[6] F. Oudet, A. Vejux, P. Courtine, Appl. Catal. 50 (1989) 79.
[7] P.C. Flynn, S.E. Wanke, J. Catal. 37 (1975) 432.
[8] P.C. Flynn, S.E. Wanke, J. Catal. 34 (1974) 390.
[9] P.C. Flynn, S.E. Wanke, J. Catal. 34 (1974) 400.
[10] H. Lieske, G. Lietz, H. Spindler, J. Völter, J. Catal. 81 (1983) 8.
[11] E. Ruckenstein, D.B. Dadyburjor, J. Catal. 48 (1977) 73.
[12] D.B. Dadyburjor, S.P. Marsh, M.E. Glicksman, J. Catal. 99 (1986) 358.
[13] H. Birgersson, L. Eriksson, M. Boutonnet, S.G. Jaras, Appl. Catal. B Environ. 54 (2004) 193.
[14] F.C. Galisteo, R. Mariscal, M.L. Granados, J.L.G. Fierro, R.A. Daley, J.A. Anderson, Appl. Catal. B Environ. 59 (2005) 227.
[15] M.J. D'Aniello, D.R. Monroe, C.J. Carr, M.H. Krueger, J. Catal. 109 (1988) 407.
[16] K. Foger, H. Jaeger, Appl. Catal. 56 (1989) 137.
[17] F.L. Normand, A. Borgna, T.F. Garetto, C.R. Apesteguia, B.D. Moraweck, J. Phys. Chem. 100 (1996) 9068.
[18] A. Monzón, T.F. Garetto, A. Borgna, Appl. Catal. A Gen. 248 (2003) 279.
[19] K. Foger, H. Jaeger, J. Catal. 92 (1985) 64.
[20] G.B. McVicker, R.L. Garten, R.T.K. Baker, J. Catal. 54 (1978) 129.

[21] Y. Nishihata, J. Mizuki, T. Akao, H. Tanaka, M. Uenishi, M. Kimura, T. Okamoto, N. Hamada, Nature 418 (2002) 164.
[22] R.M.J. Fiedorow, S.E. Wanke, J. Catal. 43 (1976) 34.
[23] T.J. Lee, Y.G. Kim, J. Catal. 90 (1984) 279.
[24] J. Adamiec, R.M.J. Fiedorow, S.E. Wanke, J. Catal. 95 (1985) 492.
[25] J.M. Rickard, L. Genovese, A. Moata, S. Nitsche, J. Catal. 121 (1990) 141.
[26] K. Otto, W.H. Weber, G.W. Graham, J.Z. Shyu, Appl. Surf. Sci. 37 (1989) 250.
[27] G. Lietz, H. Lieske, H. Spindler, W. Hanke, J. Völter, J. Catal. 81 (1983) 17.
[28] E. Ruckenstein, Y.F. Chu, J. Catal. 59 (1979) 109.
[29] I. Sushumna, E. Ruckenstein, J. Catal. 108 (1987) 77.
[30] R. Gollob, D.B. Dadyburjor, J. Catal. 68 (1981) 473.
[31] D.B. Dadyburjor, J. Catal. 57 (1979) 504.
[32] Y. Nagai, T. Hirabayashi, K. Dohmae, N. Takagi, T. Minami, H. Shinjoh, S. Matsumoto, J. Catal. 242 (2006) 103.
[33] G.A. Somorjai, Introduction to Surface Chemistry and Catalysis, John Wiley & Sons, New York, 1994, p. 388.
[34] H. Yoshida, Y. Yazawa, T. Hattori, Catal. Today 87 (2003) 19.
[35] J.A. Anderson, R.A. Daley, S.Y. Christou, A.M. Efstathiou, Appl. Catal. B Environ. 64 (2006) 189.
[36] T. Tanaka, H. Yamashita, R. Tsutitani, T. Funabiki, S. Yoshida, J. Chem. Soc. Faraday Trans. 84 (1988) 2987.
[37] A.G. McKale, B.W. Veal, A.P. Paulikas, S.K. Chan, G.S. Knapp, J. Am. Chem. Soc. 110 (1988) 3763.
[38] A. Morikawa, T. Suzuki, T. Kanazawa, K. Kikuta, A. Suda, H. Shinjoh, Appl. Catal. B Environ. 78 (2008) 210.
[39] A.N. Mansour, J.W. Cook, D.E. Sayers, J. Phys. Chem. A 88 (1984) 2330.
[40] H. Yoshida, S. Nonoyama, Y. Yazawa, T. Hattori, Phys. Scr. T 115 (2005) 813.
[41] M. Vaarkamp, Catal. Today 39 (1998) 271.
[42] A.F. Lee, K. Wilson, R.M. Lambert, C.P. Hubbard, R.G. Hurley, R.W. McCabe, H.S. Gandhi, J. Catal. 184 (1999) 491.
[43] O. Muller, R. Roy, Mater. Res. Bull. 4 (1969) 39.
[44] K. Asakura, H. Nagahiro, N. Ichikuni, Y. Iwasawa, Appl. Catal. A Gen. 188 (1999) 313.